materials

MDPI

Article

Correlation of Magnetomechanical Coupling and Damping in $Fe_{80}Si_9B_{11}$ Metallic Glass Ribbons

Xu Zhang [1,2,3,*], Yu Sun [1,2,4], Bin Yan [1,2] and Xin Zhuang [1,2,4,*]

1 Aerospace Information Research Institute, Chinese Academy of Sciences, Beijing 100190, China
2 Key Laboratory of Electromagnetic Radiation and Sensing Technology, Chinese Academy of Sciences, Beijing 100190, China
3 School of Physical Science and Technology, Inner Mongolia University, Hohhot 010021, China
4 University of Chinese Academy of Sciences, Beijing 100049, China
* Correspondence: zhangxu2019@imu.edu.cn (X.Z.); zhuangxin@aircas.ac.cn (X.Z.)

Abstract: Understanding the correlation between magnetomechanical coupling factors (k) and damping factors (Q^{-1}) is a key pathway toward enhancing the magnetomechanical power conversion efficiency in laminated magnetoelectric (ME) composites by manipulating the magnetic and mechanical properties of Fe-based amorphous metals through engineering. The k and Q^{-1} factors of FeSiB amorphous ribbons annealed in air at different temperatures are investigated. It is found that k and Q^{-1} factors are affected by both magnetic and elastic properties. The magnetic and elastic properties are characterized in terms of the magnetomechanical power efficiency for low-temperature annealing. The k and Q^{-1} of FeSiB-based epoxied laminates with different stacking numbers show that a −3 dB bandwidth and Young's modulus are expressed in terms of the magnetomechanical power efficiency for high lamination stacking.

Keywords: Fe-based amorphous alloys; magnetomechanical coupling; damping factor

1. Introduction

In recent years, Fe-based amorphous alloys with significant magnetomechanical effects have been successfully used in laminated magnetoelectric (ME) composites, which usually consist of piezoelectric and magnetostrictive layers [1–5]. The ME energy coupling of laminated piezoelectric/magnetostrictive composites can be described as magnetic energy converted to mechanical energy and then to electric energy through the strain/stress coupling between these two types of materials [2]. When a magnetic field is applied to ME composites, their ferromagnetic layers shrink or stretch due to the magnetostrictive effect; then, the resulting strain/stress is transferred to the piezoelectric material, leading to a voltage change [2]. Devices based on laminated ME structures have shown promising potential for use in magnetic sensors, acoustically driven antennas and power conversion devices due to their high energy conversion efficiency [1–4,6–11].

As a key component of ME structures, Fe-based amorphous alloys should possess a relatively high conversion efficiency between magnetic power and mechanical power. To develop such materials, the requirement is to balance two or more parameters, as relevant parameters in materials usually impact one another to a significant degree [1]. However, keeping a parameter unchanged while improving other correlated parameters is normally quite a challenging task, even more so to balance two main parameters in some energy-converting materials. Specifically, the magnetomechanical power conversion efficiency (η), defined by the ratio between the converted power and the input power and that can be expressed as $\eta = \frac{1}{1 + 1/(k^2 Q)}$ [4,12], in magnetostrictive materials is based on two mutually exclusive, but related, parameters—the magnetomechanical coupling coefficient (k) and damping factor (Q^{-1}) [2,4]. The k factor quantifies the ratio of the magnetic energy that is converted into mechanical energy or vice versa over a period in

check for updates

Citation: Zhang, X.; Sun, Y.; Yan, B.; Zhuang, X. Correlation of Magnetomechanical Coupling and Damping in $Fe_{80}Si_9B_{11}$ Metallic Glass Ribbons. *Materials* **2023**, *16*, 4990. https://doi.org/10.3390/ma16144990

Academic Editor: Matteo Cantoni

Received: 11 May 2023
Revised: 1 July 2023
Accepted: 12 July 2023
Published: 14 July 2023

magnetostrictive devices [13–15]. The Q factor, a reciprocal of the damping factor, is another important parameter that quantifies the ratio between the power storage and the power loss [12,14]. The two factors can be used to characterize the magnetomechanical properties in Fe-based amorphous alloys [4]. The k and Q factors accompany each other in most magnetomechanical transduction materials. To increase η, k^2Q needs to be maximized, although efforts to increase k often lead to a reduction in Q and vice versa. For example, the traditional annealing procedure usually causes a similar trend in changes to the k^2 and Q^{-1} factors; this implies a small η value [1,2]. To enhance the efficiency a step forward, and to minimize the inevitable correlation between the two factors, further clarity is needed on the correlation in variations between k and Q^{-1}.

Over recent decades, the influence of annealing on magnetic properties of Fe-based amorphous ribbons has been vastly studied [4,16–18]. It has been found that the annealing procedure can adjust the saturation magnetic flux density (B_s), coercivity (H_c), magnetic permeability (μ_r) and the k, Q and η factors, but variations to these parameters are rarely independent [1,4,8,11–13,19–35]. Thus, an opportunity has arisen for researchers to explore ways to cooperatively elevate two or more parameters while avoiding negatively impacting others [1–3].

In this study, the influence of heat treatment on the magnetomechanical properties for FeSiB amorphous ribbons is investigated. The correlation between the k and Q (or Q^{-1}) factors of such ribbons annealed at temperatures far below the crystallization temperature is discussed. The magnetic and magnetomechanical properties of single-foil ribbons and epoxy–ribbon laminates are also measured and compared in this work.

2. Experimental Method

The samples used in this work to perform the experiments were Fe-based amorphous ribbons with a nominal composition of $Fe_{80}Si_9B_{11}$ (at%). The length, width and thickness of a single ribbon were 40 mm, 5 mm and ~25 μm, respectively. The ribbons were annealed at different temperatures for 20 min in air using a muffle furnace. The annealed ribbons were inserted into a rectangular winding coil with an approximate size of $40 \times 10 \times 10$ mm^3 and were tightly wound into six layers using 32-AWG magnetic wires in copper. When amorphous ribbons are driven by a magnetic excitation near a mechanical resonant frequency, their impedance (and inductive component) is extremely sensitive to the applied DC field [5,7,36,37]. The inductance and the impedance of the coils with inserted ribbons were measured with a high-precision impedance analyzer (HP 4294A). The resonant frequencies ($\boldsymbol{f_r}$ at maximum impedance) and antiresonant frequencies ($\boldsymbol{f_a}$ at minimum impedance) on the impedance spectrum were also measured with the impedance analyzer under a DC magnetic bias field (H_{dc}) along the longitudinal direction of the ribbons [6,38]. It is worth mentioning that the antiresonance occurred at a frequency above the actual mechanical resonance frequency when the impedance contribution from the ribbon minimized the total impedance [12]. The values of k were determined using resonant and antiresonant frequencies, while Q could be directly measured using the two poles ($\boldsymbol{f_1}$ at maximum inductance, $\boldsymbol{f_2}$ at minimum inductance) on the inductance spectrum [4,12,38]. From the frequencies at f_r, f_a, f_1 and f_2, the values of k and Q were calculated using the following dependences: $k = \sqrt{(\pi^2/8)(1 - f_r^2/f_a^2)}$ and $Q = f_r/(f_2 - f_1)$, where $\Delta f = f_2 - f_1$ also corresponds to the -3 dB bandwidth near the resonance [12]. A schematic diagram of the experiment is shown in Figure 1.

The magnetic permeability μ_r of the Fe-based amorphous ribbon was an order of 10^4–10^5 [39]. When cut into the rectangular shape, the apparent magnetic permeability (μ_{app}) along the long axis of the ribbon was several hundred due to the demagnetization field [40]. Furthermore, because the inductance of the winding coil was almost constant for a fixed frequency, this caused the measured inductance (L) values of the winding coil with an inserted Fe-based ribbon to increase with the increase in μ_{app}, i.e., $L \propto \mu_{app}$.The values of Young's modulus (E) for the ribbons with lengths matching the coils' should have been approximately proportional to the square of *the* antiresonant frequency f_a or the square of the resonant frequency f_r [12,14,34], i.e., $E \propto f_a^2 (or\ f_r^2)$. The magnetic hysteresis loops of the ribbons annealed at different temperatures were measured using the vibrational sample measurement system (VSM, MicroSense EZ-7). The samples with dimensions of approximately $5 \times 5 \times 0.025$ mm^3 were prepared together in a furnace with the 40 mm long ribbons for the VSM measurements.

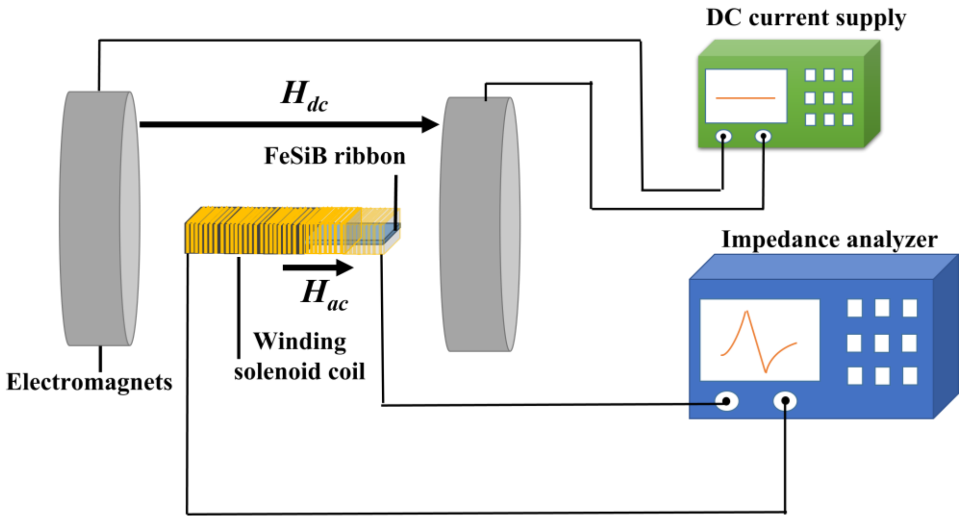

Figure 1. Schematic diagram of the experiment.

3. Theoretical Analysis and Measurement

3.1. Eddy Current Loss

The equivalent input loss factor (ξ) is defined as the inverse of the product of k^2 and Q. It quantifies the ratio between the power conversion and the power loss in the magnetic-to-mechanical energy conversion. Following previous investigations [4,12,32,34,41], ξ could be written as

$$\xi = \frac{1}{k^2 Q} = c_e \mu_0 \chi f_r + \frac{1}{k^2 Q_0}, \tag{1}$$

where c_e is the loss coefficient for the eddy current in an individual ribbon, χ is the magnetic susceptibility of the ribbons and Q_0 is the quality factor under magnetostriction-free conditions. From the right-hand side of Equation (1), the first term c_e represents the energy loss for the dynamic magnetization procedure, which was affected by the magnetic properties of the ribbon; the second part represents loss not related to the eddy current. In single ribbons, the eddy current loss dominated after the heat treatment under an annealing temperature far below the crystallization temperature. Following Herzer et al. [42], the formula for c_e was expressed as

$$c_e = \frac{(\pi t)^2}{6\rho_{el}} \left(1 + \frac{w^2}{(w cos\beta + t)^2} \frac{m^2}{1 - m^2}\right), \tag{2}$$

where t is the ribbon thickness, ρ_{el} is the electric resistivity and β is the angle between the average magnetic anisotropy and the ribbon direction. $m = J_H / J_s$ is the average longitudinal magnetization (J_H) normalized to the saturation magnetization (J_S). w is the magnetic domain width; the formula was given as [42]

$$w^2 = \frac{8 L_{ex} t}{N_{zz} sin^2\beta + N_{yy} cos^2\beta}, \tag{3}$$

where $L_{ex} = \sqrt{A/K}$ is the magnetic exchange length. A is defined as the exchange stiffness and K is the anisotropy constant. N_{zz} and N_{yy} are the demagnetization factors along the longitudinal and width directions of the ribbon, respectively. With the help of Equations (2) and (3), the contribution of the eddy current in Equation (1) could be rewritten as

$$\xi_{eddy} = \frac{(\pi t)^2}{6\rho_{el}}\mu_0\chi f_r + \frac{(\pi t)^2}{6\rho_{el}}\frac{m^2}{1-m^2}\frac{w^2}{(wcos\beta + t)^2}\mu_0\chi f_r. \quad (4)$$

Taking into account that the average anisotropy angle β was close to zero for ribbons annealed at low temperatures, Equation (4) was rewritten as

$$\xi_{eddy} = \frac{(\pi t)^2}{6\rho_{el}}\mu_0\chi f_r + \frac{\pi^2}{6\rho_{el}}\frac{m^2}{1-m^2}\left(\frac{1}{t}+\frac{1}{w}\right)^{-2}\mu_0\chi f_r. \quad (5)$$

Since the magnetic domain width was usually much larger than the ribbon thickness in low-temperature annealed samples, the assumption $w >> t$ could be considered in the calculation. Thus, Equation (5) could be rewritten as

$$\xi_{eddy} = \frac{1}{k^2 Q} = \frac{(\pi t)^2}{6\rho_{el}}\left(1+\frac{m^2}{1-m^2}\right)\mu_0\chi f_r. \quad (6)$$

The equivalent loss factor induced by the eddy current loss for the ribbons annealed at low temperature was dominated by the variation in χ and f_r for the ribbons.

3.2. Magnetic and Magnetomechanical Properties

It was assumed that the hysteresis loops of the magnetic materials could provide important information on the magnetic properties of the materials. Figure 2a shows the DC magnetic hysteresis loops of the samples annealed in air at different annealing temperatures (T_{AN}) for 20 min. The loops showed small values of remnant magnetization and H_c for all the samples, suggesting that the samples retained good soft magnetic properties after the heat treatment in air. As shown in the inset in Figure 2a, the values of H_c mostly stayed close to 0.1 Oe for T_{AN} = 370 °C to 450 °C. However, H_c began to grow sharply when T_{AN} exceeded 450 °C. In this case, the change in the chemical concentration causing the ordered clusters and the subsequent topological and chemical long-range orderings on the surfaces of the ribbons resulted in variations in the values of H_c [28,30,31,33,41,43]. When T_{AN} was above 500 °C, H_c showed a high increase, which suggested further deterioration in the soft magnetic properties. This was due to (1) an increase in the fraction of the surface crystallization at high T_{AN} and (2) the film of boron oxides that formed due to the excessive presence of boron atoms that were separated from the α-Fe crystallites, since the α-Fe crystallites had a much lower solubility effect on B than that of amorphous Fe [4,22,27,28,30,33]. Consequently, the magnetic domains in the amorphous remainders were thinned and turned toward the out-of-plane direction through compression stress induced by the surface crystallization and surface oxidation films [4,22,27,28,30,33], leading to an increasing in H_c.

In our previous work [4], we reported on the T_{AN} dependency of k and Q for single FeSiB ribbons; the value of k reached its maximum at approximately a T_{AN} of 430 °C, while Q showed a minimal value at approximately a T_{AN} of 410 °C. The k^2 and Q^{-1} evolutions after annealing at various temperatures T_{AN} are shown in Figure 2b. In the low T_{AN} region, below 400 °C, with increasing T_{AN}, both k^2 and Q^{-1} increased at almost the same pace, indicating that k^2 and Q^{-1} were correlated in the low annealing temperature region. For higher T_{AN}, from 400 °C to 500 °C, the variation in k^2 and Q^{-1} diverged, suggesting that the correlation level of the two parameters dropped significantly. Furthermore, as a result of the collective changes in k^2 and Q^{-1} for low T_{AN}, below 400 °C, the equivalent input loss ξ should have stayed invariable for low T_{AN}, below 400 °C, as reported by our earlier investigations [4].

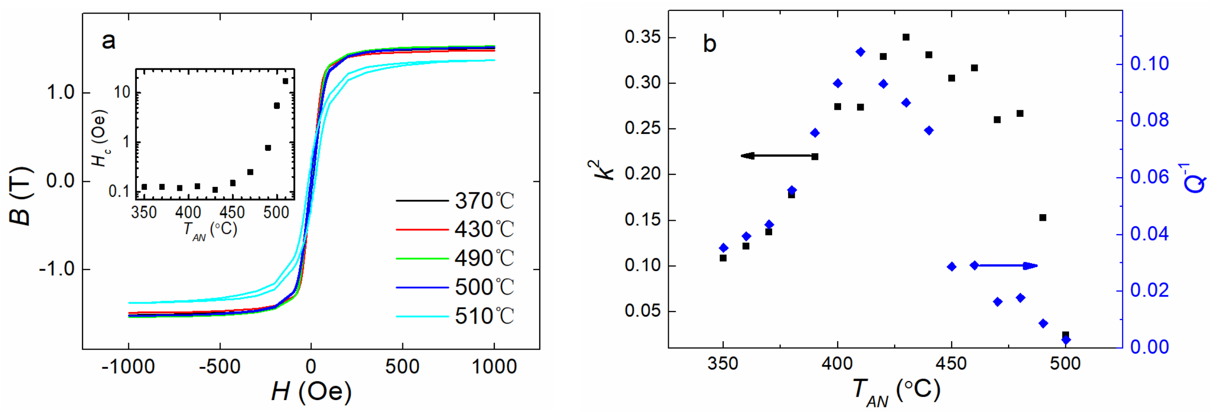

Figure 2. (**a**) The hysteresis loops of FeSiB amorphous ribbons obtained after annealed at different temperatures, from 370 °C to 510 °C, for 20 min in air; the inset figure is the annealing temperature (T_{AN}) dependence of coercivity H_c. (**b**) Damping factors (Q^{-1}) and the square of magnetomechanical coupling (k) as a function of T_{AN} for 20 min in air. k was acquired at its maximal values with external DC magnetic bias field H_{dc}. The values of Q^{-1} were measured under the same H_{dc} when k was maximized.

3.3. Softening of Magnetic and Elastic Properties

Figure 3 shows the measured values of the inductance (L) at 10 kHz after isothermal annealing at various temperatures T_{AN}. It could be observed that L increased with T_{AN} in the region from 350 °C to 410 °C and then decreased for T_{AN} from 420 °C to 490 °C. As mentioned above in the Section 2, the variation in L values suggested a collective change in the apparent magnetic permeability (μ_{app}) of the ribbon [44], i.e., $L \propto \mu_{app}$.

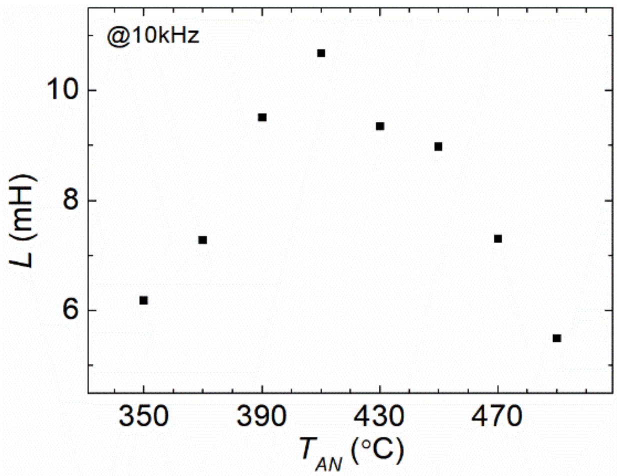

Figure 3. Variations in inductance (L) of the winding coil with an inserted FeSiB ribbon annealed for 20 min at different annealing temperatures T_{AN}, from 350 °C to 490 °C.

Figure 4 shows the T_{AN} dependence of resonant f_r and antiresonant f_a. It could be stated that in the low T_{AN} region, both f_r and f_a decreased with the increase in T_{AN}, reaching a minimal value at 410 °C. Then, they rose as T_{AN} continued to increase. The values of Young's modulus (E) in the ribbons with lengths matching those of the coils should have been approximately proportional to the square of *the* antiresonant frequency f_a or the square of the resonant frequency f_r [12,14,34], i.e., $E \propto f_a^2 (or\ f_r^2)$. By comparing the behavior of L and f_a (f_r) versus T_{AN}, it could be seen that the two parameters exhibited a respective extreme value as the function of T_{AN}. However, the curves of L and f_a (f_r) showed a lag of 20 °C versus T_{AN} to reach their maximum/minimum values.

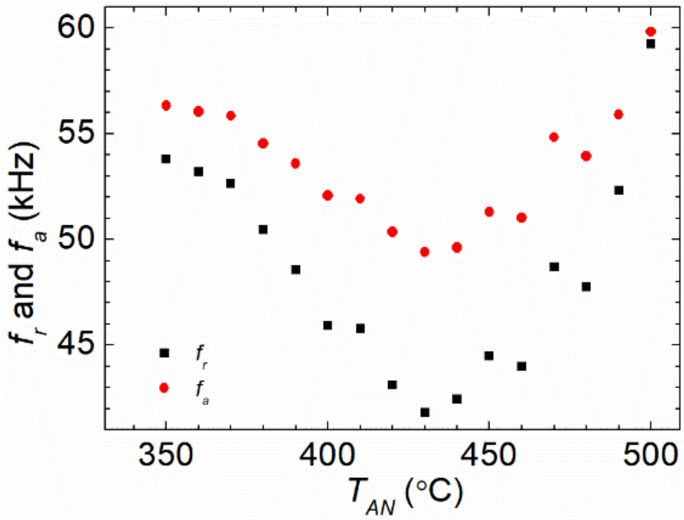

Figure 4. The variation in the resonant frequencies (f_r) and antiresonant frequencies (f_a) of the winding coil with an inserted FeSiB ribbon annealed for 20 min at different annealing temperatures T_{AN}, from 350 °C to 500 °C. The f_r and f_a on the motion impedance curve were measured with the impedance analyzer under a DC magnetic bias field (H_{dc}) along the longitudinal direction of the ribbons.

By comparing the T_{AN} dependence of L with the T_{AN} dependence of the Q^{-1} factors, it could be observed that the variations in L and Q^{-1} with the increase in T_{AN} were almost the same below 400 °C; f_a (f_r) had a similar profile to the k factor. According to Equation (6), the trends of k and Q were recognized as the competition between the magnetic and mechanical properties, χ and f_a (f_r). Since the L curve and Q^{-1} curve shared the same trend and the same extreme value point of T_{AN} below 410 °C while the f_a (f_r) curve and the k curve showed an inverse trend and the same extreme value point of T_{AN} below 430 °C, it was probable that L or μ_{app} were dominant in the values of the Q^{-1} factors, while f_a (f_r) or E had a dominative effect on the k factor for the low T_{AN} below 410 °C (for L and Q) or 430 °C (for f_a and k). Moreover, because k and E were related to each other, the annealing experience through α relaxation had a significant influence on the softening of elasticity below 430 °C [4]. For higher T_{AN}, because of the emergence of the surface crystallization and the long-range chemical orderings with B oxidation during the annealing procedure, the competition of magnetism and elasticity became much more complex, leading to the divergence between the k^2 curve and Q curves, as well as between the f_a (f_r) curve and the L curve versus T_{AN} [4,28,30,31,33,35,41].

Below 410 °C-T_{AN}, the β relaxation in the Fe-deficient zones was dominant and led to the chemical short-range ordering (CSRO) in Fe-rich zones with doped B atoms through diffusion [4]. In addition, the topological short-range ordering (TSRO) also occurred at this low T_{AN} region as another result of β relaxation, leading to the release of internal stress, both of which weakened the pinning effect of the magnetic domain through defects in the sample [4]. The expanding speed of the magnetic domain increased, therefore, i.e., L (μ_{app}) increased. For T_{AN}, from 450 °C to 500 °C, the sharp decrease in L (μ_{app}) may have occurred due to the emergence of surface crystallization together with more severe surface oxidation (such as Fe-O, B-O, silica) that led to the appearance of the grain boundary, as well as the magnetic anisotropy deviating from the long axis direction, both of which inhibited the movement or rotation of the magnetic moment of the magnetic domain, resulting in the smaller variation rate of the magnetic moment. The increase in H_c above 450 °C also coincided with the decrease in L (μ_{app}), suggesting the deterioration of the soft magnetic properties in the high T_{AN} region.

The decrease in E in the low T_{AN} region suggested that the deformation quantity of the ribbon decreased with the increasing T_{AN}. According to previous studies [4,35], as a result of β relaxation for low T_{AN}, besides the increase in the Fe–Fe bond caused by the CSRO, the TSRO could also be triggered through β relaxation close to the cluster–matrix boundaries.

The TSRO initiated a decrease in the ductility of the sample; thus, the sample became "more flexible" when stretched. Consequently, E (f_a and f_r) decreased after annealing at a relatively low temperature, and reached its minimum at 430 °C, as shown in Figure 4. The E (f_a and f_r) vs. T_{AN} curve switched to an increasing trend when T_{AN} exceeded 430 °C. This could be attributed to the apparency of α relaxation, which was more intense and usually occurred at a high T_{AN}. This α relaxation further enhanced the diffusion of the atoms, affecting the atomic orderings in a larger scale and usually reshaping the clusters. Fe or metalloid atoms experiencing long-term relaxation in the B-rich area led to the generation of some clusters with high elasticity, which increased the values of E. In addition, because the annealing procedure in this article was performed in air, the oxidation was stronger and penetrated deeper into the ribbons at a high T_{AN}; this also had a strong influence on the rigidity of the ribbon [4,20].

From Figures 3 and 4, it could be obtained that the variation trends in magnetic susceptibility χ (χ was also approximately proportional to L in Figure 3) and resonant (antiresonant) frequency f_r (f_a) were quite similar, but opposite for low T_{AN} from 350 °C to 400 °C; the product of χ and f_r (f_a) remained close to the constant. Moreover, the measured η, relating to k^2Q, was nearly a constant value in this region of T_{AN}, following our previous investigations [4,8]. Therefore, according to Equation (1), it could be inferred that the loss factor c_e that represented the eddy current loss should have been mostly unchanged for low T_{AN} from 350 °C to 400 °C for the single FeSiB ribbons. This was consistent with our analysis in the theoretical section as well.

When T_{AN} approached the crystallization temperature (T_x) of the FeSiB glassy metals, the size of the magnetic domain decreased due to the change in surface stress [4,31,33]. According to Herzer et al. [4,12,32,34,41,43], the loss factor c_e is related to the width of the magnetic domain w, following Equation (2). Therefore, the collectively changing behavior of k^2 and Q^{-1} suggested that the improvement in the soft magnetic properties may have derived from the increase in the number of activated magnetic units rather than variations in the width of the magnetic domains in the low T_{AN} region. Thus, the values of ξ for the ribbons annealed at low T_{AN} remaining constant had more to do with the increase in the quantity of magnetic units rather than the change in the domain size.

3.4. Time–Temperature Equivalence for Annealing

Figure 5a,b display the variations in the k, k^2Q and Q factors for different annealing times t_{AN} at T_{AN} ranging from 470 °C to 490 °C, respectively. A significant decrease in the k factor with the increase in the Q factor occurred with the increase in t_{AN} for a T_{AN} of 470 °C and 490 °C. The curve for k and Q showed a cross profile at t_{AN} = 40 min and 15 min, respectively. After the ribbons were annealed for 40 min at T_{AN} = 470 °C and 15 min at T_{AN} = 490 °C, k decreased from approximately 60% to 40%, while the values for Q increased close to 200. The equivalent input loss factors ξ showed a maximum value when the t_{AN} was 20 min for both samples, which suggested the optimal annealing time (20 min) for annealing at 470 °C and 490 °C. Based on the data mentioned above, it was implied that the decrease in k was caused by the surface oxidation and surface crystallization that induced the increase in coercivity through the out-of-plane magnetic anisotropy. The increase in Q factors might have been due to the long-range orderings that took place on the surface regions of the ribbons.

The Q factor represents the quality of mechanical performance in our FeSiB ribbons; a high value in the Q factor indicates a high ratio between the storage power and power loss. Figure 5a,b show that the overall trend of the k, k^2Q and Q curves at 470 °C T_{AN} was similar to that at 490 °C T_{AN}, separately. Moreover, the increase in T_{AN} from 470 °C to 490 °C narrowed the T_{AN} window before the magnetomechanical performance visibly deteriorated. In terms of the η factors, it was similar to the increase in T_{AN} for a constant t_{AN} or to increase in t_{AN} at a fixed T_{AN}, which suggested that T_{AN} and t_{AN} had an equal effect on the η factor in the heat treatment procedure for the FeSiB ribbons to some extent. However, the equivalence of t_{AN} and T_{AN} in terms of the magnetomechanical power conversion efficiency seemed to exist only at relatively higher T_{AN}; we did not observe this equivalent with T_{AN} below 400 °C.

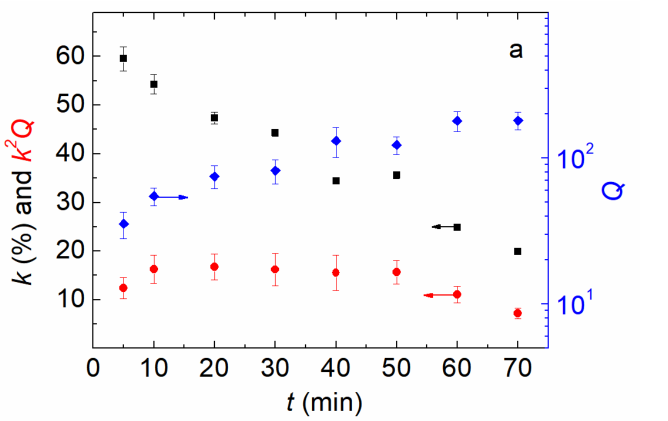

Figure 5. The magnetomechanical coupling coefficient (k) for FeSiB ribbons as a function of the annealing time (t_{AN}) at annealing temperature of (**a**) 470 °C and (**b**) 490 °C. The blue and red curves represent the values of the quality factors (Q) and efficiency factors (k^2Q) associated with the maximum values of coupling coefficient k, respectively.

3.5. Magnetomechanical Properties in Epoxy–Ribbon Composites

A schematic diagram of a laminated composite consisting of magnetostrictive amorphous FeSiB ribbons bonded with epoxy resin is given in Figure 6a. Several FeSiB foils were fabricated using hot-pressing techniques and an A–B part epoxy. The ratio between the epoxy (A part) and the curing agent (B part) should be 3:1, but in this case the curing part is a little bit less than the should-be value. Figure 6b is a photo of the laminated FeSiB composites; we applied a DC magnetic field along the laminated composite, as shown in the upper part of Figure 6b. The ratio between the quantity of the magnetostrictive layers and the quantity of epoxy resin varied during the investigation of the changes in k, Q and k^2Q in the FeSiB laminated composites with different foil numbers. The results are given in Figure 7a. It was found that as the number of FeSiB layers increased, the k factors increased slightly and then decreased rapidly, while the Q factors showed an overall increasing trend to a maximum close to 400, corresponding to a foil number from 18 to 21 in the FeSiB laminates. The efficiency factor k^2Q first increased in the presence of more FeSiB ribbon layers and then reached a relatively stable value at approximately 25, corresponding to an FeSiB foil number from 12 to 21. Figure 7b shows the trend of the −3 dB bandwidth (Δf) and E for the FeSiB laminated composites with different foil numbers.

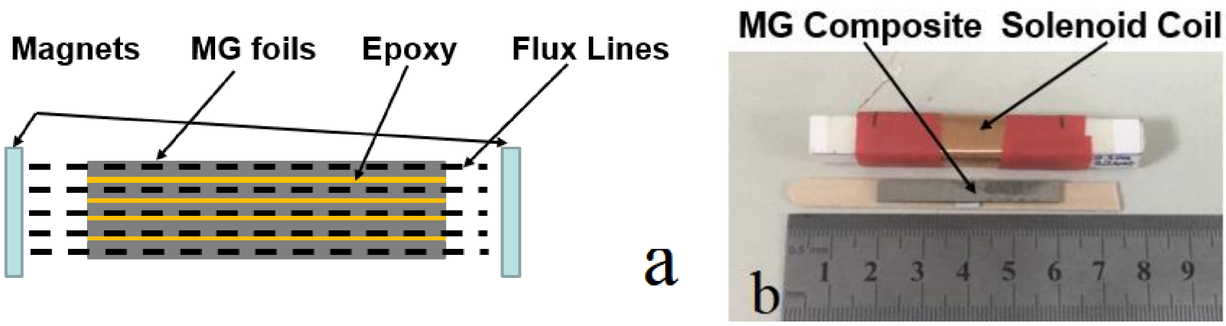

Figure 6. (**a**) Schematic diagram of a laminated composite consisting of magnetostrictive amorphous FeSiB ribbons bonded with epoxy resin. (**b**) Photo of laminated metallic glass (FeSiB) ribbon composites and the winding coil used to generate the AC magnetic field.

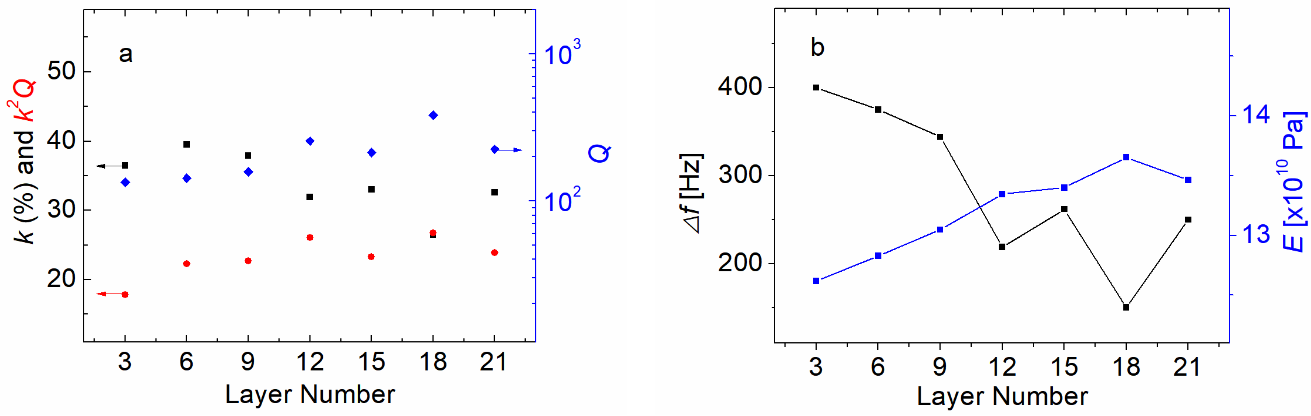

Figure 7. (**a**) The black curve is the magnetomechanical coupling factor (k) for laminated metallic glass composites consisting of magnetostrictive amorphous FeSiB ribbons as a function of the FeSiB layer number. The blue and red curves represent the values of the quality factors (Q) and efficiency coefficients (k^2Q) associated with the maximum values of coupling coefficient k, respectively. (**b**) The trend of the -3 dB bandwidth (Δf) and Young's modulus (E) for laminated FeSiB ribbon composites as a function of the FeSiB layer number, where $\Delta f = f_2 - f_1$ (f_1 at maximum inductance, f_2 at minimum inductance).

In Figure 7a, it was observed that when the foil number was small, there was no obvious similarity or correlation between the k and Q factors as the FeSiB layer number varied. The k and Q in the laminated composites with nine layers, six layers and three layers of FeSiB ribbons were examples. However, for the laminated composites with more foil number of 12 layers, 15 layers, 18 layers and 21 layers, the data suggest that there was a mutually exclusive relationship between the k and Q factors. This caused the k^2Q factors to reach a relatively stable state, while the k^2Q factors did not continue to increase with the increase in FeSiB layers. For the record, we needed to particularly emphasize that the ratio between the epoxy and curing agents was *not* 3:1. The amount of curing agent was reduced, giving a ratio of more than 3:1 between the epoxy and the curing agent, so the epoxy resin was not fully solidified for the laminated samples. Thus, the mechanical loss due to the interfriction increased compared to the samples with fully cured epoxy. Unlike the eddy current loss in the single-foil ribbons, the dominant loss in the FeSiB laminates was ascribed to the mechanical loss that triggered the temperature rise when the laminated composites were driven under high-power conditions.

According to previous research [4,31], as T_{AN} approached T_x, the size of the magnetic domain decreased due to the change in surface stress. As mentioned above, the efficiency of a single-foil ribbon experienced a low T_{AN} that remained constant, and this was more due to the increase in the number of magnetic units rather than the change in the magnetic domain size. In contrast, the increase in the k^2Q factors at T_{AN} above 450 °C was due to the reduction in magnetic domain size. Following Equation (1), because the k^2Q factors of the laminated FeSiB composites were approximately constant for a high layer number of laminates, and because the variation trend of E (associated with f_r and f_a) and the bandwidth (associated with χ) of the laminated FeSiB composites remained consistent with each other for all the foil numbers, the c_e of the laminated composites should have also remained unchanged. As the foil number of the FeSiB laminates decreased, the volume proportion of magnetostrictive materials (FeSiB) in the laminated composite gradually increased. Using a similar analysis principle to Figure 7a, the reason for the constant values in the k^2Q factors for the ribbons with foil numbers ranging from 12 to 21 was probably due to the increase in the number of ribbons rather than the change in the relative fraction of the ribbons. The reason for the change in the k^2Q factors for the laminates with foil numbers ranging from 3 to 12 was due to the variation in the relative volume fraction of FeSiB ribbons rather than a variation in the ribbon number. This indicated that the change in the k^2Q factors between the laminates with ribbon numbers ranging from 3 to 12 derived from the relative size of the magnetic units, which probably corresponded to the relative volume fraction of the FeSiB ribbons in the laminates, while the constant k^2Q factors between the 12-layer and 21-layer laminates might have arisen from the change in the number of magnetic units rather than the change in the relative volume of magnetic units [45].

4. Conclusions

In summary, we investigated the influence of magnetic and elastic properties on magnetomechanical coupling factors (k) and damping factors (Q^{-1}) by measuring the resonant and antiresonant frequencies from the motion impedance and inductance spectrum of a winding coil with an annealed FeSiB ribbon. We could draw the following conclusions:

1. Through annealing under different temperatures, it was found that the dynamic magnetic and elastic properties in the $Fe_{80}Si_9B_{11}$ ribbons varied correlatively with the annealing temperature. However, the resonant frequency reached its minimum value at 430 °C, with a lag of 20 °C, when the magnetic parameter reached its minimum at 410 °C, coinciding with the behaviors of k and Q^{-1} when the annealing temperature changed.

2. It was found that the annealing temperature and annealing time equally impacted the heat treatment procedure for the FeSiB ribbons in maximizing the magnetomechanical power efficiency. However, the equivalence was correct only when the annealing temperature was high enough for the long-range orderings to occur on the surface region of the ribbons.

3. For the FeSiB laminated composites, when the foil number ranged from 12 to 21, the trends of k and Q were synchronously related but opposite. This suggested that the behavior of the k and Q factors in the laminates with foil numbers ranging from 12 to 21 was at some point in analogy with the behaviors of the k and Q^{-1} factors in the single-foil FeSiB ribbons with various annealing temperatures ranging from 350 °C to 400 °C.

Author Contributions: Conceptualization, X.Z. (Xin Zhuang); methodology, X.Z. (Xin Zhuang) and X.Z. (Xu Zhang); software, X.Z. (Xin Zhuang) and X.Z. (Xu Zhang); validation, X.Z. (Xin Zhuang) and X.Z. (Xu Zhang); formal analysis, X.Z. (Xin Zhuang) and X.Z. (Xu Zhang); investigation, X.Z. (Xin Zhuang) and X.Z. (Xu Zhang); resources, X.Z. (Xin Zhuang) and X.Z. (Xu Zhang); data curation, X.Z. (Xin Zhuang) and X.Z. (Xu Zhang); writing—original draft preparation, X.Z. (Xu Zhang); writing—review and editing, X.Z. (Xin Zhuang), X.Z. (Xu Zhang), Y.S. and B.Y.; visualization, X.Z. (Xin Zhuang) and X.Z. (Xu Zhang); supervision, X.Z. (Xin Zhuang); project administration, X.Z. (Xin Zhuang) and X.Z. (Xu Zhang); funding acquisition, X.Z. (Xin Zhuang) and X.Z. (Xu Zhang). All authors have read and agreed to the published version of the manuscript.

Funding: This research was funded by the National Key R & D Program of China, no. 2021YFA0716500, the Natural Science Fund of Inner Mongolia Autonomous Region, no. 2021BS05010, and the talent program with the Chinese Academy of Sciences.

Institutional Review Board Statement: Not applicable.

Informed Consent Statement: Not applicable.

Data Availability Statement: Not applicable.

Conflicts of Interest: The authors declare no conflict of interest.

References

1. Channagoudra, G.; Dayal, V. Magnetoelectric Coupling in Ferromagnetic/Ferroelectric Heterostructures: A Survey and Perspective. *J. Alloys Compd.* **2022**, *928*, 167181. [CrossRef]
2. Leung, C.M.; Li, J.; Viehland, D.; Zhuang, X. A Review on Applications of Magnetoelectric Composites: From Heterostructural Uncooled Magnetic Sensors, Energy Harvesters to Highly Efficient Power Converters. *J. Phys. D Appl. Phys.* **2018**, *51*, 263002. [CrossRef]
3. Narita, F.; Fox, M. A Review on Piezoelectric, Magnetostrictive, and Magnetoelectric Materials and Device Technologies for Energy Harvesting Applications. *Adv. Eng. Mater.* **2018**, *20*, 1700743. [CrossRef]
4. Zhuang, X.; Xu, X.; Zhang, X.; Sun, Y.; Yan, B.; Liu, L.; Lu, Y.; Zhu, W.; Fang, G. Tailoring the Magnetomechanical Power Efficiency of Metallic Glasses for Magneto-Electric Devices. *J. Appl. Phys.* **2022**, *132*, 104502. [CrossRef]

5. Gutiérrez, J.; Barandiarán, J.M.; Nielsen, O.V. Magnetoelastic Properties of Some Fe-Rich Fe-Co-Si-B Metallic Glasses. *Phys. Status Solid* **1989**, *111*, 279–283. [CrossRef]
6. Leung, C.M.; Zhuang, X.; Xu, J.; Li, J.; Zhang, J.; Srinivasan, G.; Viehland, D. Enhanced Tunability of Magneto-Impedance and Magneto-Capacitance in Annealed Metglas/PZT Magnetoelectric Composites. *AIP Adv.* **2017**, *8*, 055803. [CrossRef]
7. Stoyanov, P.G.; Grimes, C.A. A Remote Query Magnetostrictive Viscosity Sensor. *Sens. Actuators A Phys.* **2000**, *80*, 8–14. [CrossRef]
8. Sun, Y.; Zhang, X.; Wu, S.; Zhuang, X.; Yan, B.; Zhu, W.; Dolabdjian, C.; Fang, G. Magnetomechanical Properties of Fe-Si-B and Fe-Co-Si-B Metallic Glasses by Various Annealing Temperatures for Actuation Applications. *Sensors* **2023**, *23*, 299. [CrossRef]
9. Qiao, K.; Hu, F.; Zhang, H.; Yu, Z.; Liu, X.; Liang, Y.; Long, Y.; Wang, J.; Sun, J.; Zhao, T.; et al. Unipolar Electric-Field-Controlled Nonvolatile Multistate Magnetic Memory in FeRh/(001)PMN-PT Heterostructures over a Broad Temperature Span. *Sci. China Phys. Mech. Astron.* **2021**, *65*, 217511. [CrossRef]
10. Pal, M.; Srinivas, A.; Asthana, S. Enhanced Magneto-Electric Properties and Magnetodielectric Effect in Lead-Free (1-x)$0.94Na_{0.5}Bi_{0.5}TiO_3$-$0.06BaTiO_3$–x $CoFe_2O_4$ Particulate Composites. *J. Alloys Compd.* **2022**, *900*, 163487. [CrossRef]
11. Li, T.X.; Li, R.; Lin, Y.; Bu, F.; Li, J.; Li, K.; Hu, Z.; Ju, L. Study of Enhanced Magnetoelectric Coupling Behavior in Asymmetrical Bilayered Multiferroic Heterostructure with Two Resonance Modes. *J. Alloys Compd.* **2022**, *895*, 162674. [CrossRef]
12. Kaczkowski, Z. Magnetomechanical Properties of Rapidly Quenched Materials. *Mater. Sci. Eng. A* **1997**, *226–228*, 614–625. [CrossRef]
13. Kabacoff, L.T. Thermal, Magnetic, and Magnetomechanical Properties of Metglas 2605 S2 and S3. *J. Appl. Phys.* **1982**, *53*, 8098–8100. [CrossRef]
14. Savage, H.; Clark, A.; Powers, J. Magnetomechanical Coupling and ΔE Effect in Highly Magnetostrictive Rare Earth—Fe_2compounds. *IEEE Trans. Magn.* **1975**, *11*, 1355–1357. [CrossRef]
15. Kaczkowski, Z.; Vlasák, G.; Švec, P.; Duhaj, P. Magnetostriction and Magnetomechanical Coupling of Heat-Treated Fe54Ni20Nb3Cu1Si13B9 Metallic Glass. *Mater. Sci. Eng. A* **2004**, *375–377*, 1062–1064. [CrossRef]
16. Chen, H.S.; Leamy, H.J.; Barmatz, M. The Elastic and Anelastic Behavior of a Metallic Glass. *J. Non Cryst. Solids* **1971**, *5*, 444–448. [CrossRef]
17. Morito, N.; Egami, T. Correlation of the Shear Modulus and Internal Friction in the Reversible Structural Relaxation of a Glassy Metal. *J. Non Cryst. Solids* **1984**, *61–62*, 973–978. [CrossRef]
18. Soshiroda, T.; Koiwa, M.; Masumoto, T. The Internal Friction and Elastic Modulus of Amorphous Pd–Si and Fe–P–C Alloys. *J. Non Cryst. Solids* **1976**, *22*, 173–187. [CrossRef]
19. Xu, D.D.; Zhou, B.L.; Wang, Q.Q.; Zhou, J.; Yang, W.M.; Yuan, C.C.; Xue, L.; Fan, X.D.; Ma, L.Q.; Shen, B.L. Effects of Cr Addition on Thermal Stability, Soft Magnetic Properties and Corrosion Resistance of FeSiB Amorphous Alloys. *Corros. Sci.* **2018**, *138*, 20–27. [CrossRef]
20. Lin, J.; Li, X.; Zhou, S.; Zhang, Q.; Li, Z.; Wang, M.; Shi, G.; Wang, L.; Zhang, G. Effects of Heat Treatment in Air on Soft Magnetic Properties of FeCoSiBPC Amorphous Core. *J. Non Cryst. Solids* **2022**, *597*, 121932. [CrossRef]
21. Murugaiyan, P.; Mitra, A.; Jena, P.S.M.; Mahato, B.; Ghosh, M.; Roy, R.K.; Panda, A.K. Grain Refinement in Fe-Rich FeSiB(P)NbCu Nanocomposite Alloys through P Compositional Modulation. *Mater. Lett.* **2021**, *295*, 129852. [CrossRef]
22. Fang, Z.; Nagato, K.; Liu, S.; Sugita, N.; Nakao, M. Investigation into Surface Integrity and Magnetic Property of FeSiB Metallic Glass in Two-Dimensional Cutting. *J. Manuf. Process.* **2021**, *64*, 1098–1104. [CrossRef]
23. Wang, C.; Guo, Z.; Wang, J.; Sun, H.; Chen, D.; Chen, W.; Liu, X. Industry-Oriented Fe-Based Amorphous Soft Magnetic Composites with SiO_2-Coated Layer by One-Pot High-Efficient Synthesis Method. *J. Magn. Magn. Mater.* **2020**, *509*, 166924. [CrossRef]
24. Cheng, Y.Q.; Ma, E. Atomic-Level Structure and Structure-Property Relationship in Metallic Glasses. *Prog. Mater. Sci.* **2011**, *56*, 379–473. [CrossRef]
25. Czyż, O.; Kusiński, J.; Radziszewska, A.; Liao, Z.; Zschech, E.; Kąc, M.; Ostrowski, R. Study of Structure and Properties of Fe-Based Amorphous Ribbons after Pulsed Laser Interference Heating. *J. Mater. Eng. Perform.* **2020**, *29*, 6277–6285. [CrossRef]
26. Zhang, J.; Shan, G.; Li, J.; Wang, Y.; Shek, C.H. Structures and Physical Properties of Two Magnetic Fe-Based Metallic Glasses. *J. Alloys Compd.* **2018**, *747*, 636–639. [CrossRef]
27. Li, Y.; Chen, W.-Z.; Dong, B.-S.; Zhou, S.-X. Effects of Phosphorus and Carbon Content on the Surface Tension of FeSiBPC Glass-Forming Alloy Melts. *J. Non Cryst. Solids* **2018**, *496*, 13–17. [CrossRef]
28. Lopatina, E.; Soldatov, I.; Budinsky, V.; Marsilius, M.; Schultz, L.; Herzer, G.; Schäfer, R. Surface Crystallization and Magnetic Properties of Fe84.3Cu0.7Si4B8P3 Soft Magnetic Ribbons. *Acta Mater.* **2015**, *96*, 10–17. [CrossRef]
29. Ok, H.N.; Morrish, A.H. Origin of the Perpendicular Anisotropy in Amorphous Fe82B12Si6 Ribbons. *Phys. Rev. B* **1981**, *23*, 2257–2261. [CrossRef]
30. Gemperle, R.; Kraus, L.; Kroupa, F.; Schneider, J. Influence of Surface Oxidization on Induced Anisotropy of Amorphous (FeNi) PB Wires. *Phys. Status Solidi (a)* **1980**, *60*, 265–272. [CrossRef]
31. Ok, H.N.; Morrish, A.H. Amorphous-to-Crystalline Transformation of Fe82B12Si6. *Phys. Rev. B* **1980**, *22*, 3471–3480. [CrossRef]
32. Keupers, A.; De Schepper, L.; Knuyt, G.; Stals, L.M. Chemical and Topological Short Range Order in Amorphous Fe40Ni38Mo4B18 (Metglas 2826MB). *J. Non Cryst. Solids* **1985**, *72*, 267–278. [CrossRef]
33. Morito, N. Surface Crystallization Induced by Selective Oxidation of Boron in Fe-B-Si Amorphous Alloy. *Key Eng. Mater.* **1990**, *40–41*, 63–68. [CrossRef]

34. Herzer, G. Magnetomechanical Damping in Amorphous Ribbons with Uniaxial Anisotropy. *Mater. Sci. Eng. A* **1997**, *226–228*, 631–635. [CrossRef]
35. Tong, X.; Zhang, Y.; Wang, Y.; Liang, X.; Zhang, K.; Zhang, F.; Cai, Y.; Ke, H.; Wang, G.; Shen, J.; et al. Structural Origin of Magnetic Softening in a Fe-Based Amorphous Alloy upon Annealing. *J. Mater. Sci. Technol.* **2022**, *96*, 233–240. [CrossRef]
36. Herrero-Gómez, C.; Marín, P.; Hernando, A. Bias Free Magnetomechanical Coupling on Magnetic Microwires for Sensing Applications. *Appl. Phys. Lett.* **2013**, *103*, 142414. [CrossRef]
37. Hernando, A.; Madurga, V.; Barandiarán, J.M.; Liniers, M. Anomalous Eddy Currents in Magnetostrictive Amorphous Ferromagnets: A Large Contribution from Magnetoelastic Effects. *J. Magn. Magn. Mater.* **1982**, *28*, 109–116. [CrossRef]
38. Kaczkowski, Z.; Vlasák, G.; Švec, P.; Duhaj, P.; Ruuskanen, P.; Barandiarán, J.M.; Gutiérrez, J.; Minguez, P. Influence of Heat-Treatment on Magnetic, Magnetostrictive and Piezomagnetic Properties and Structure of Fe64Ni10Nb3Cu1Si13B9 Metallic Glass. *Mater. Sci. Eng. A* **2004**, *375–377*, 1065–1068. [CrossRef]
39. Herzer, G. Modern Soft Magnets: Amorphous and Nanocrystalline Materials. *Acta Mater.* **2013**, *61*, 718–734. [CrossRef]
40. Séran, H.C.; Fergeau, P. An Optimized Low-Frequency Three-Axis Search Coil Magnetometer for Space Research. *Rev. Sci. Instrum.* **2005**, *76*, 044502. [CrossRef]
41. Egami, T. Structural Relaxation in Amorphous Fe40Ni40P14 B6 Studied by Energy Dispersive X-ray Diffraction. *J. Mater. Sci.* **1978**, *13*, 2587–2599. [CrossRef]
42. Herzer, G. Effect of Domain Size on the Magneto-Elastic Damping in Amorphous Ferromagnetic Metals. *Int. J. Mater. Res.* **2022**, *93*, 978–982. [CrossRef]
43. Egami, T. Structural Relaxation in Amorphous Alloys—Compositional Short Range Ordering. *Mater. Res. Bull.* **1978**, *13*, 557–562. [CrossRef]
44. Setiadi, R.N.; Schilling, M. Sideband Sensitivity of Fluxgate Sensors Theory and Experiment. *Sens. Actuators A Phys.* **2019**, *285*, 573–580. [CrossRef]
45. Hasegawa, R.; Ramanan, V.R.V.; Fish, G.E. Effects of Crystalline Precipitates on the Soft Magnetic Properties of Metallic Glasses. *J. Appl. Phys.* **1982**, *53*, 2276–2278. [CrossRef]